A VARIATIONAL APPROACH TO EXPLOIT PRIOR INFORMATION IN OBJECT-BACKGROUND SEGREGATION: APPLICATION TO RETINAL IMAGES

Luca Bertelli, Jiyun Byun, B. S. Manjunath

Center for BioImage Informatics
Department of Electrical and Computer Engineering
University of California, Santa Barbara, CA 93106
{lbertelli, jiyun, manj}@ece.ucsb.edu

ABSTRACT

One of the main challenges in image segmentation is to adapt prior knowledge about the objects/regions that are likely to be present in an image, in order to obtain more precise detection and recognition. Typical applications of such knowledge-based segmentation include partitioning satellite images and microscopy images, where the context is generally well defined. In particular, we present an approach that exploits the knowledge about foreground and background information given in a reference image, in segmenting images containing similar objects or regions. This problem is presented within a variational framework, where cost functions based on pairwise pixel similarities are minimized. This is perhaps one of the first attempts in using non-shape based prior information within a segmentation framework. We validate the proposed method to segment the outer nuclear layer (ONL) in retinal images. This approach successfully segments the ONL within an image and enables further quantitative analysis.

Index Terms— Region-based image segmentation, variational methods, level sets, bioimage analysis.

1. INTRODUCTION

Object-background segregation can be considered as the combination of two different, but tightly coupled, subtasks: object detection and segmentation. Most of the general purpose segmentation techniques, such as active contours [1], region growing or watersheds [2, 3], and spectral methods [4], are generally not suitable for separating a particular object from a cluttered background. Shape information, extensively used in the literature (see [5] and references therein), is not suitable to describe complex objects, such as in biological images.

This paper presents a segmentation method, which exploits the prior knowledge in the form of a reference image with known background/object separation. We define variational cost functions using a dissimilarity measure between pixels of the reference image and pixels of the images to be segmented. The minimization of these cost functions is achieved within a level set framework, resulting in a combined recognition and segmentation of the objects of interest.

We demonstrate the utility of the proposed approach on confocal microscopy images of retina taken during detachment experiments. Retinal images are critical components for understanding the structural and cellular changes of a retina in response to detachment. The first step towards any further advanced analysis is to have a reliable map of the retinal layers. Segmenting retinal images is often difficult because of their unique challenges. Image data in an individual region (e.g. layer) is not statistically homogeneous. Further difficulties in retinal images include visual variation from staining and considerable variation of the object (layer) shape (see Section 3 for more details). In this context, retinal images are perfect datasets to validate the proposed method. The objects of interest here are different retinal layers (such as the ONL in Fig. 3), that we aim to separate from the rest of the layers.

The rest of paper is organized as follows. In Section 2, we introduce novel variational cost functions to include prior information in the object-background segmentation process and we minimize these cost functions within a level set framework. Section 3 specializes the approach to segment the ONL from the retinal images. Experimental results are discussed in Section 4 and we briefly conclude in Section 5.

2. OBJECT/BACKGROUND SEGMENTATION USING DISSIMILARITIES WITH A REFERENCE

Consider an image I_1 and a reference image I_2. We assume known a partitioning of the reference image in foreground F_2 and multiple components of the background B_{2i}, with $i = 1 \dots n$. We propose to segregate the foreground in I_1, namely F_1, from its background B_1 by minimizing the following cost function:

$$E = \sum_{p_1 \in F_1} \sum_{p_2 \in F_2} w(p_1, p_2) + \sum_{p_1 \in B_1} \min_i \sum_{p_2 \in B_{2i}} w(p_1, p_2) \quad (1)$$

This work was supported by NSF ITR-0331697. We would like to thank Dr. Geoffery Lewis and prof. Steven Fisher from the Neuroscience Research Institute for the retinal image dataset and Eden Haven for ground truth.

where $w(p_1, p_2)$ is a dissimilarity measure between pixels $p_1 \in I_1$ and $p_2 \in I_2$. F_1, B_1 are a partitioning of I_1 such that $F_1 \cup B_1 = I_1$ and similarly F_2, B_{2i} are a partitioning of the reference I_2 such that $F_2 \cup \bigcup_{i=1}^{n} B_{2i} = I_2$. In order to minimize the cost function in (1) within a variational framework, we rewrite it in a continuous domain formulation as:

$$E = \int_{I_1}\int_{I_2} w(p_1,p_2)\chi_{F_1}(p_1)\chi_{F_2}(p_2)dp_2dp_1 + \int_{I_1}\min_i \int_{I_2} w(p_1,p_2)\chi_{B_1}(p_1)\chi_{B_{2i}}(p_2)dp_2dp_1 \quad (2)$$

where

$$\chi_{F_1}(p) = \begin{cases} 1 & \text{if } p \in F_1 \\ 0 & \text{if } p \notin F_1 \end{cases}$$

and χ_{F_2}, χ_{B_1}, $\chi_{B_{2i}}$ are defined in a similar way. Since χ_{F_2} and $\chi_{B_{2i}}$, with $i = 1 \ldots n$, are fixed, we need to minimize (2) with respect to χ_{F_1} and χ_{B_1}. We are now going to represent χ_{F_1} and χ_{B_1} within a level set framework. Define a 3D surface ϕ such that $F_1 = \{p_1 \in I_1 \mid \phi(p_1) > 0\}$ and $B_1 = \{p_1 \in I_1 \mid \phi(p_1) < 0\}$. It is now possible to rewrite (2) as:

$$E(\phi) = \int_{I_1}\int_{I_2} w(p_1,p_2)H(\phi(p_1))\chi_{F_2}(p_2)dp_2dp_1 + \int_{I_1}\min_i \int_{I_2} w(p_1,p_2)\Big(1 - H(\phi(p_1))\Big)\chi_{B_{2i}}(p_2)dp_2dp_1 \quad (3)$$

where the Heaviside function $H(z)$ is equal to 1 if $z > 0$ and 0 if $z < 0$. The gradient projection method minimizing $\int f(\phi(x))dx$, using t as the descent variable leads to:

$$\frac{\partial \phi}{\partial t} = -\frac{\partial f}{\partial \phi} \quad (4)$$

In our case we can manipulate (3) so that:

$$f(\phi(p_1)) = \int_{I_2} w(p_1,p_2)H(\phi(p_1))\chi_{F_2}(p_2)dp_2 + \min_i \int_{I_2} w(p_1,p_2)\Big(1 - H(\phi(p_1))\Big)\chi_{B_{2i}}(p_2)dp_2 \quad (5)$$

Therefore, applying (4) to (5) yields the curve evolution for ϕ, which minimizes $E(\phi)$:

$$\frac{\partial \phi(p_1)}{\partial t} = \delta(\phi(p_1))\Big[-\int_{I_2} w(p_1,p_2)\chi_{F_2}(p_2)dp_2 + \min_i \int_{I_2} w(p_1,p_2)\chi_{B_{2i}}(p_2)dp_2\Big] \quad (6)$$

The cost function in (1) is biased towards equal sized partitions. To remove this bias we normalize (6) as follows:

$$\frac{\partial \phi(p_1)}{\partial t} = \delta(\phi(p_1))\Big[\frac{-1}{|\chi_{F_2}|}\int_{I_2} w(p_1,p_2)\chi_{F_2}(p_2)dp_2 + \min_i \frac{1}{|\chi_{B_{2i}}|}\int_{I_2} w(p_1,p_2)\chi_{B_{2i}}(p_2)dp_2\Big] \quad (7)$$

where $|\chi| = \int \chi(p)dp$, *i.e.* the area of the region represented by the characteristic function χ. Every point on the zero level set curve of ϕ in I_1 is compared in similarity with the foreground F_2 of the reference and with the part of that background (B_{2i}) that is less dissimilar with. The curve is then expanded or shrunk accordingly, including or excluding that point from the emerging foreground F_1. A regularization term is needed in the cost function to prevent the curve from wrapping around spurious noisy regions. This is done by adding a term proportional to the length of the zero level set of ϕ (see [6, 1]):

$$E_L = \mu \int_{I_1} |\nabla H(\phi(p_1))|dp_1 \quad (8)$$

Minimizing (8) via the steepest descent, we obtain a motion by mean curvature equation for ϕ:

$$\frac{\partial \phi(p_1)}{\partial t} = \mu\, \delta(\phi(p_1))\mathrm{div}\Big(\frac{\nabla\phi(p_1)}{|\nabla\phi(p_1)|}\Big) \quad (9)$$

The right hand side of (9) has to be added to the right hand side of (7) to obtain the complete curve evolution for ϕ.

3. RETINAL LAYERS SEGMENTATION

A vertical section of a retina illustrates its complexity and highly patterned architecture (Fig. 1). Each retinal layer has a different structure consisting of the group of cell bodies or synaptic terminals. Changes in the integrity of the layers, such as deformations of the layer boundaries and cell densities, serve as an index of retinal function after injury. Moreover, this layer information is used for localizing specific cells and analyzing the effects of genes or drugs on retinal integrity. Of interest to biology are measures such as the number of cell, the layer thickness and changes in protein distribution in each layer. Hence retinal layer segmentation is a critical first step in quantifying the effects of retinal detachment or injury.

Since confocal retinal images are generated by using fluorescence, only specific regions where fluorescent dye molecules bind are visualized. The tissue stained with an antibody is collected as a pseudo colored image. High intensity in the image corresponds to a high concentration of protein expression and the rest of an image appears as dark regions (Fig. 2 (a)). When the tissue is stained with multiple antibodies, the response to each antibody is combined to form a color image where the color represents the protein response to each antibody. In addition, each layer has a different cellular structure, which result in specific texture patterns as shown in Fig. 2 (b).

Consider Fig.3 that shows a reference image I_2. The layer marked as ~~ONL~~ in this image is our reference foreground F_2. We would like to segment out this layer from the rest of the images in our collection. Other layers in the reference image will form the background set $\{B_{2i}\}$. Note that the layer ML in Fig 3 consists of four different layers that are not visually distinguishable from each other. From a retinal biology view

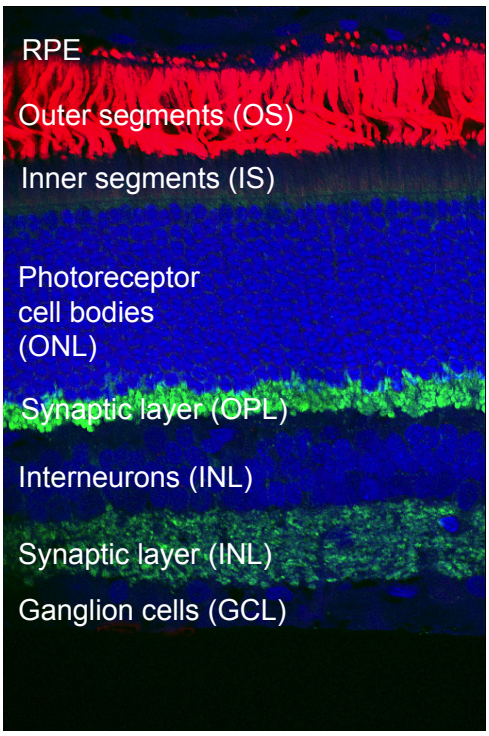

Fig. 1. Confocal microscopy of a vertical section through a cat retina.

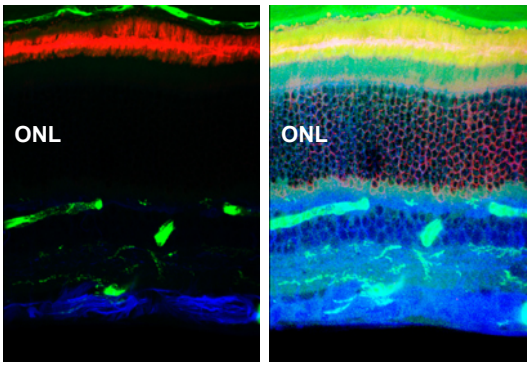

(a) (b)

Fig. 2. Example retinal images. (a) Triple labeled image of rod photoreceptors (anti-rod opsin; red), microglia (isolectin B4; green), and Müller cells (anti-GFAP; blue). (b) Histogram equalized image of (a).

point it is important to identify the ONL which serves as a baseline for the cellular changes under a degenerative condition and in identifying the other layers. Therefore we focus on segmenting the ONL.

4. EXPERIMENTAL RESULTS

We present the result of applying proposed method to a series of confocal images. 50 images of cat retina were generated

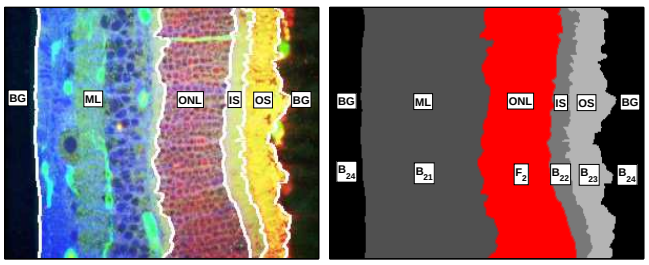

(a) (b)

Fig. 3. Application to retinal images. (a) A reference image. The layer boundaries are manually created. (b) Foreground F_2 (red) and multiple components of the background B_{2i} (gray levels) as in equation (7).

from tissue sections under four different experimental conditions: 10 normal, 14 1-day, 14 3-day, and 7-day detached. Images were labeled with isolectin B4 (green) and with antibodies to rod opsin (red) and GFAP (blue) (Fig. 2). The image of 1-day detached retina shown in Fig. 3 is used as a reference to segment the ONL from all 50 images. The ground truth data, consisting of the boundaries for the ONL, is created manually.

The dissimilarity measure $w(p_1, p_2)$ are computed as linear combination of color and texture information. Specifically:

$$w(p_1, p_2) = \alpha\, w_{col}(p_1, p_2) + (1 - \alpha)\, w_{tex}(p_1, p_2), \quad (10)$$

where $w_{col}(p_1, p_2) = \left(\sum_{i=1}^{3}(c_i(p_1) - c_i(p_2))^2\right)^{1/2}$ is the distance between pixels in the space defined by three antibody channels c_i, and $w_{tex}(p_1, p_2) = \left(\sum_{i=1}^{30}(t_i(p_1) - t_i(p_2))^2\right)^{1/2}$ is the distance in the space defined by the Gabor filter outputs [7], evaluated at five scales and six orientations (t_i represents the output at one particular scale and orientation).

The curve evolution for equation (7+9) is implemented using a semi-implicit finite difference scheme with the curvature coefficient $\mu = 2000$ for all the experiments. Fig. 4 shows the some of the visual segmentation results of images under four different conditions ($\alpha = 0.5$). The detected ONL boundaries are depicted in white and the ground truth in black.

In order to provide a quantitative evaluation of the results, we ~~compared~~ them with the ground truth, computing *precision* (p) and *recall* (r) as measures of the accuracy of the segmentation[1]. In Fig. 5 (a) present the *F measure*, the harmonic mean of precision and recall ($F = \frac{2pr}{p+r}$), varying the parameter α (weight of color and texture features). The best score $F = 0.883$ is obtained for $\alpha = 0.5$, which means equal weight for color and texture. Since using only color information the performance does not degrade significantly ($F = 0.873$ for $\alpha = 1$), the texture information can be neglected, if saving in computation time is necessary.

[1]Precision is the probability that a pixel, indicated as belonging to the ONL by the segmentation algorithm, is truly on ONL pixel. Recall is the probability that an ONL pixel is correctly detected by the algorithm

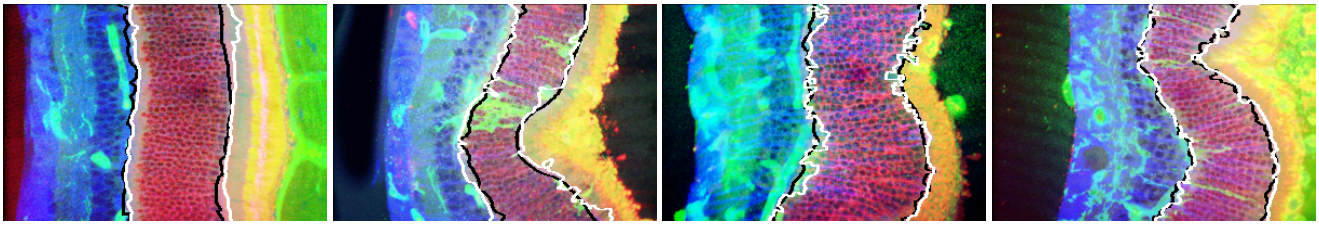

(a) (b) (c) (d)

Fig. 4. Segmentation results using $\alpha = 0.5$. The white boundaries are detected by the proposed algorithm and black ones are ground truth. (a) Normal (b) 1 day after detachment (c) 3 days after detachment (d) 7 days after detachment. In (b) and (d), despite the presence of lectin-labeled cells (green objects), the ONL boundaries are delineated correctly.

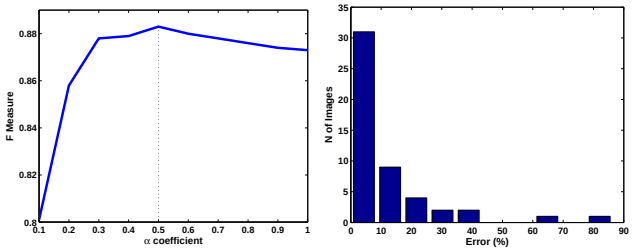

(a) (b)

Fig. 5. Quantitative evaluation of the results. (a) F measures varying the parameter α for the segmentation of the 50 images. (b) Error distribution using nuclei detection.

To validate if the segmentation results can be used for further analysis, we compute the nuclei density within the segmented region in an image using [8] (for $\alpha = 0.5$). The nuclei density is then compared with the density computed using the ground truth (manually segmented boundaries). The average error is 11.4% ranging with about 50 % of the images having less than 5 % of error. The error distribution is shown in Fig. 5 (b) (there were a few outlier images with large errors, which are mostly attributed to poor imaging conditions). We also ~~evaluated~~ the precision and recall using the number of detected nuclei within the ONL (as opposed as pixels within the ONL) and the resulting F measure is 0.92. Overall the proposed method results in high quality segmentation of the ONL ~~i~~ that would not have been possible without using prior information. We are currently working on evaluating the segmentation performance on the remaining layers as well.

5. CONCLUSIONS

We introduced a variational framework to exploit prior information in the foreground/bacgkround segmentation. Exploiting the knowledge about foreground and background in a reference image, we defined a dissimilarity measure between the pixels of the reference and the pixel of the image to be segmented. We defined a variational cost function based on these dissimilarities and we minimized it within a level set framework. We ~~demonstrate~~ a successful segmentation of the ONL in retinal images[2]. The segmented results are immediately useful for further analysis including counting nuclei of photoreceptors within the ONL. Improved version of the proposed model for object-background segmentation in cluttered natural images is part of the future work.

6. REFERENCES

[1] T. F. Chan and L. A. Vese, "Active contours without edges," *IEEE Transactions on Image Processing*, pp. 266–77, February 2001.

[2] S. C. Zhu and A. Yuille, "Region competition: unifying snakes, region growing, and bayes/mdl for multiband image segmentation," *IEEE Transactions on PAMI*, pp. 884–900, Sep 1996.

[3] L. Vincent and P. Soille, "Watersheds in digital spaces: an efficient algorithm based on immersion simulations," *IEEE Transactions on PAMI*, pp. 583–598, June 1991.

[4] J. Shi and J. Malik, "Normalized cuts and image segmentation," *IEEE Transactions on PAMI*, pp. 888–905, August 2000.

[5] D. Cremers, "Dynamical statistical shape priors for level set based tracking," *IEEE Transactions on PAMI*, vol. 28, no. 8, pp. 1262–1273, August 2006.

[6] S. Osher and J. A. Sethian, "Fronts propagating with curvature-dependent speed: Algorithms based on hamilton-jacobi formulations," *Journal of Computational Physics*, vol. 79, pp. 12–49, 1988.

[7] B. S. Manjunath and W. Y. Ma, "Texture features for browsing and retrieval of image data," *IEEE Transactions on PAMI*, pp. 837–42, August 1996.

[8] J. Byun, M. R. Verardo, B. Sumengen, G. P. Lewis, B. S. Manjunath, and S. K. Fisher, "Automated tool for the detection of cell nuclei in digital microscopic images: Application to retinal images," *Molecular Vision*, vol. 12, pp. 949–960, Aug 2006.

[2]More examples and data set with ground truth are available at http://bioimage.ucsb.edu/retina_segmentation.php.